Analytica Chimica Acta 1117 (2020) 25–34

Contents lists available at ScienceDirect

Analytica Chimica Acta

journal homepage: www.elsevier.com/locate/aca

A fabrication strategy for protein sensors based on an electroactive molecularly imprinted polymer: Cases of bovine serum albumin and trypsin sensing

Wei Zhao [a], Bing Li [a], Sheng Xu [a], Ye Zhu [b, **], Xiaoya Liu [a, *]

[a] Key Laboratory of Synthetic and Biological Colloids, Ministry of Education, School of Chemical and Material Engineering, Jiangnan University, Wuxi, Jiangsu Province, 214122, PR China

[b] International Joint Research Center for Photoresponsive Molecules and Materials, Jiangnan University, 1800 Lihu Avenue, Wuxi, Jiangsu Province, 214122, PR China

HIGHLIGHTS

- A novel electroactive molecularly imprinted interface was developed as an abiotic recognition with high generality.
- A linear amphipathic macromolecule was designed as macro-monomer to maintain structural integrity of the protein template.
- The sensing platform was based on an enhanced electron transfer mechanism after the generation of an electroactive network.
- Bovine serum albumin (BSA) and trypsin were used as model proteins to investigate the method's generality.

GRAPHICAL ABSTRACT

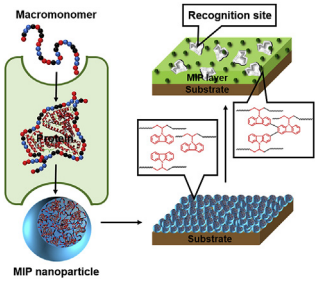

ARTICLE INFO

Article history:
Received 15 December 2019
Received in revised form
9 April 2020
Accepted 10 April 2020
Available online 13 April 2020

Keywords:
Molecularly imprinted polymer
Self-assembly
Protein recognition
Electrochemistry

ABSTRACT

A high-performance molecularly imprinted sensing platform inspired by natural recognition mechanisms was fabricated to detect protein by employing a linear electro-polymerizable molecularly imprinted polymer as macromonomer. This was achieved via the combination of a biosensor fabrication with a self-assembly imprinting technique without the use of chemical labels. An amphipathic electroactive copolymer was designed as macro-monomer to maintain structural integrity of the protein template via self-assembly, resulting in generation of a 3D construction around the protein molecule to form imprinted sites. Electro-polymerization was utilized not only to anchor imprinted sites but also to enhance electron transfer. The adaptable sensing platform was based on a strengthened recognition reaction between the MIP layer and template protein after the generation of an electroactive network. Bovine serum albumin (BSA) and trypsin were used as model proteins to investigate the method's generality, which gave broad detection ranges of 10^{-14}–10^{-5} mg mL^{-1} for BSA and 10^{-13}–10^{-8} mg mL^{-1} for trypsin. These results indicate that the proposed fabrication offers an effective and versatile strategy for protein recognition.

* Corresponding author.
** Corresponding author.
E-mail addresses: zhuye@jiangnan.edu.cn (Y. Zhu), lxy@jiangnan.edu.cn (X. Liu).

https://doi.org/10.1016/j.aca.2020.04.023
0003-2670/

1. Introduction

Nature is a resource offering great inspiration for materials science, which can be used to develop technologies in both engineering and theoretical fields [1,2]. This multitude of enlightenments has always promoted scientists to exploit and understand advanced materials and devices, which can improve our day-to-day life. "Biomimetic materials" can be defined as intelligent functional materials designed in a biomimetic way, and much focus has been applied to the evolution of this kind of materials with novel properties [3]. Molecular recognition, one of the most critical features in nature, is of great importance in biomimetic materials [4]. Over the last few decades, strategies have achieved molecular recognition *in vitro*. For instance, bio-enzymes and DNA nanotechnology have provided unparalleled precision and programmability for specific target recognition [5], and structure-based ligands (e.g., cyclodextrin, cucurbituril, calixarene) can rely on host-guest combinations to identify and quantify weak noncovalent interactions [6]. However, the effectiveness of these custom materials with recognition functions are limited by current methodologies, such as difficulty to keep the enzyme activity and high cost. On this limitation, molecularly imprinted polymers (MIPs) could offer short preparation time and relatively easy conditions for synthesis.

MIP design has been inspired by the well-known "induced fit" model [7]. It is generally dubbed as "artificial antibody", that can open new perspectives for promising recognition capability, rapid manufacture, and reasonable cost [8]. In general, target molecules can act as the template which pre-assemble with functional monomers via covalent/non-covalent interactions. The polymerization of functional monomers and crosslinkers occurs to construct a 3D network around template molecules. After the removal of template molecules, antibody-like binding sites can be generated in the polymeric matrix, which is complementary with size, shape, and structured orientation of the template [9]. The ability of MIP to recognize the template is comparable to the sensitivity and affinity of natural recognition elements. Over the past few decades, MIP has been researched and applied in the areas of catalysis [10], environmental treatments [11], solid phase extraction [12], drug delivery [13], and sensors. As a significant application, sensors based on MIPs have drawn a great attention in microgravimetric [14], electrochemical [15], optical [16] and thermal [17] platforms.

A critical point when optimizing recognition performance of MIPs is in the construction of an effective imprinted interface with rapid mass-transfer efficiency, fast rebinding speed and good selectivity, especially for biomacromolecule templates. In comparison to small templates, the imprints of biomacromolecule or proteins are still facing enormous challenges due to their large sizes with conformational flexibility and high surface complexity [18]. There have been various strategies to synthesize protein imprinted polymers, such as overall imprinting [19], surface imprinting [20], and epitope-mediated imprinting [21]. Nevertheless, a critical limitation is that most of these polymerization methods require toxic reagents for initiation, resulting in impurities from by-products or initiators in the obtained MIPs. These unnecessary moieties can significantly influence the performance of MIPs [22]. In addition, biomacromolecules are easily permeated by conventionally small monomers and crosslinkers used in the imprinting procedure, which disrupts internal hydrogen bonds and native conformation of biomacromolecules [18]. In terms of this issue, it is highly expected that if biomacromolecule templates can be imprinted by macromolecular monomers to avoid protein degeneration. This can provide a novel strategy to fabricate MIPs for biomacromolecules recognition, as well as a practical improvement in methodology.

More importantly, in the conventional sense, synthetic MIPs are insulative and inactive, giving inferior responsiveness in comparison with enzymes. To help solve this problem, conductive materials such as gold/silver nanoparticles or carbon nanotubes have been incorporated into MIPs to improve electron transfer [23,24]. Results have demonstrated that this is an effective method to enhance the recognition performance of MIPs. However, recent research shows that there is no evidence to support the universally acknowledged claims of direct electron transfer between recognition element and conductive nanomaterials [25]. Hence, it is highly supposed that if electro-active units can be introduced intrinsically to allow internal electron transfer in MIPs, further enhancement of signal conversion can be achieved. This will be a fundamental improvement in the design of high-performance MIP materials.

Self-assembly, ubiquitous in organisms, offers a bottom-up way to the fabrication of new materials [26]. By a noncovalent fashion to organize building blocks precisely, nature utilizes it to create complex functional materials and systems [27]. Recently, utilizing this versatile strategy, our group have fabricated an adaptable approach to construct nano-scaled MIPs in aqueous solution, in which post-polymerizable amphiphilic random copolymers can be designed as building blocks to imprint different small-molecular templates [23,24]. Vast amounts of results have indicated that it is effective for MIP fabrication. Inspired by this, a highly versatile molecularly imprinted sensing platform was fabricated innovatively to recognize protein via self-assembly of a linear electropolymerizable MIP as macro-monomer (Scheme 1). Rather than using inert small monomers to synthesize MIP, linear macromolecular chains as macro-monomers were employed to protect the protein template's structural integrity. In this process, a selected protein was encapsulated into nano-aggregations driving by noncovalent interaction to generate self-assembled MIP nanoparticles. Then the resultant nanoparticles can be immobilized onto a substrate and electro-polymerization was used to generate electroactive network. After template removal, a high-efficiency MIP sensor was obtained for electrochemical protein recognition. This strategy is supposed to be applied to other proteins as a versatile and universal sensing platform. This study testifies that it is one of the most effective strategies to recognize protein with high generality.

2. Experimental section

2.1. Materials and characterization

Acrylamide (AM), 2-hydroxyethyl acrylate (HEA), N-vinyl carbazole (Nvc), 2,2-azobisisobutyronitrile (AIBN), bovine serum albumin (BSA), trypsin, ovalbumin (OVA) and bovine hemoglobin (BHB) were obtained from Aladdin Chemical Reagent Co., Ltd. (Shanghai, China). Tryptophan (Tryp), lysine (Lys), L-glutamic acid (Glu), glycine (Gly), N, N-dimethylformamide (DMF), acetone, sodium dodecyl sulfate (SDS), acetic acid, $K_3[Fe(CN)_6]$, KCl, $K_4[Fe(CN)_6]$, $LiClO_4$, acetonitrile (ACN), dibasic sodium phosphate, and sodium dihydrogen phosphate (analytical grade) were purchased from Sinopharm Chemical Reagent Co., Ltd. (Shanghai, China). All solutions were prepared with ultra-pure water (18.2 MΩ cm), produced by a NW Ultra-pure Water System.

Characterization and measurements are described in the Supplementary Information.

2.2. Synthesis of the electro-polymerizable amphiphilic macromonomer Poly(AM-co-HEA-co-NVc) (PAHN)

The electro-polymerizable macro-monomer PAHN was synthesized according to Scheme 2. Simply using one-pot free radical polymerization in N_2 atmosphere, acrylamide (AM, 50 mmol), 2-

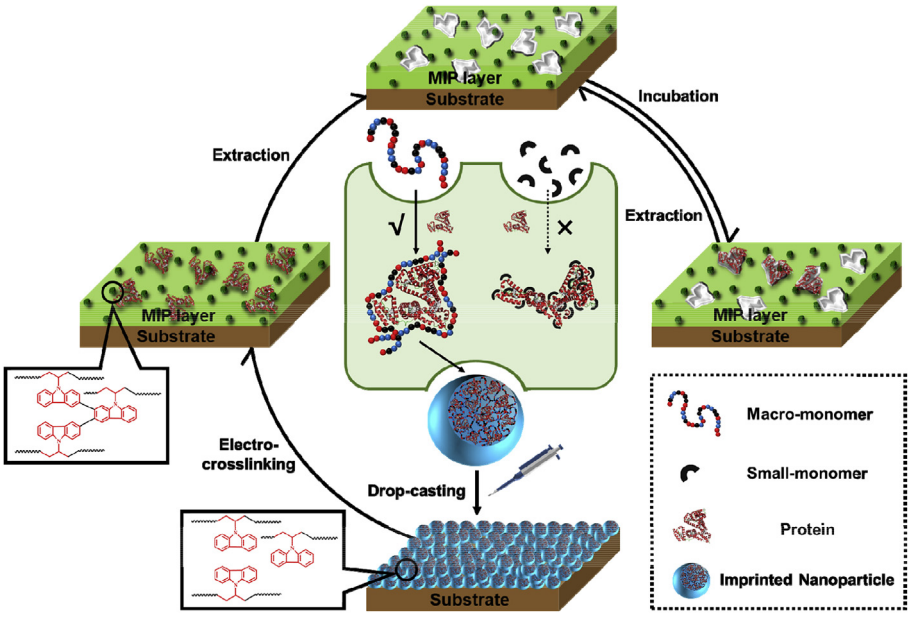

Scheme 1. Schematic representation of high-efficiency imprinted sensing platform via self-assembly of electroactive polymer as macro-monomer.

hydroxyethyl acrylate (HEA, 50 mmol) and N-vinyl carbazole (NVc, 50 mmol) were copolymerized in DMF for 24 h, initiated by 2,2-azobisisobutyronitrile (AIBN). The resultant solution was precipitated into acetone for 3 times, then dialyzed against deionized water. Finally, PAHN can be obtained as white powder after freeze-drying.

2.3. Preparation of protein imprinted polymeric nanoparticles (MIP NPs)

It is a simple way to generate water-dispersive MIP NPs. PAHN copolymer (1 mg) was dissolved in DMF (1 mL) firstly to obtain a homogenous solution. Bovine serum albumin (BSA, 66 kDa) was selected as a model protein template. Newly prepared aqueous BSA (0.5 mL, 0.5 mg mL^{-1}) was added dropwise, and the mixed solution was keeping stirring for 12 h. Whereafter, some ultrapure water (0.5 mL) was added at a rate of 10 μL s^{-1} with stirring. Then the MIP NPs aqueous dispersion was formed after dialyzing against ultrapure water to remove DMF. Non-imprinted nanoparticles (NIP NPs) were prepared similarly but in the absence of BSA. Otherwise, trypsin was employed as another template to prepare trypsin imprinted nanoparticle.

2.4. Fabrication of MIP electrochemical sensor (MIP sensor)

As shown in Scheme 1, simple drop-casting method was used to prepare protein imprinted sensor. 10 μL MIP aqueous dispersion was drop-casted onto the surface of a cleaned gold electrode. Then it was air-dried, resulting in formation of MIP NP-modified electrode. The MIP layer was electrochemically polymerized using cyclic voltammetry (CV) technology in an acetonitrile (ACN) solution with 0.1 M $LiClO_4$, and then the electrode was washed thoroughly with ultrapure water. The protein template was extracted by a mixture of SDS/acetic acid (10% w/v:10% v/v).

3. Results and discussion

3.1. Characterization of the electro-polymerizable amphiphilic macro-monomer Poly(AM-co-HEA-co-NVc) (PAHN)

The macro-monomer poly(AM-*co*-HEA-*co*-NVc) (PAHN) was designed to imprint protein in aqueous solution. Basic features are considered to obtain optimal recognition performance. Firstly, multiple hydrogen-bonding should be established easily between the macro-monomer and template protein. This is the key to ensure the success and effectiveness of non-covalent imprinting. Secondly, the macro-monomer should be amphipathic to ensure satisfactory dispersion stability in aqueous solution, which enables the co-assembly of macro-monomer with template molecules to form nano-aggregations. Finally, electroactive units are required to be post-polymerized, not only to construct a robust MIP network with a suitable crosslinking degree, but to also give the final MIP intrinsic electroactivity. Considering these structural requirements, PAHN was synthesized according to Scheme 2. Herein, acrylamide (AM)

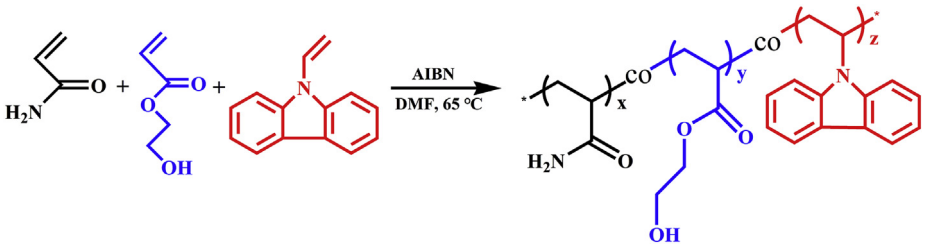

Scheme 2. Synthetic route of electro-polymerizable amphiphilic macro-monomer Poly(AM-*co*-HEA-*co*-NVc) (PAHN).

was employed as protein affinity moieties for its well-acknowledged interaction with biomolecules [28], and N-vinyl carbazole (NVc) was chosen as a hydrophobic and electro-active unit that could be electrochemically polymerized through carbazole self-oxidation [29]. The third group 2-hydroxyethyl acrylate (HEA) was used to increase the flexibility of the polymer chain and improve the film-forming properties [30]. With all features considered, the structure and characteristics of pre-designed PAHN should be in favor of protein imprinting.

^{1}H NMR spectrum and FT-IR spectrum was performed to investigate the structure of PAHN (Fig. 1). In ^{1}H NMR spectrum, the signal at 8.5–7.0 ppm represents the protons of NVc units and amidogen in AM. The chemical shifts from 4.0 to 1.0 ppm are owing to methylene protons in HEA and polymer skeleton. The hydroxy proton in HEA is assigned to 4.6 ppm. In FT-IR spectrum, the peaks at 3342 cm^{-1} correspond to N–H stretching vibration in AM units and O–H in HEA; 2933 cm^{-1} are related to C–H stretching vibration; 1722 cm^{-1} and 1662 cm^{-1} are related to the stretching vibration of C=O bond; a peak at 1075 cm^{-1} corresponds to C–N stretching vibration, and the peaks at 1452 cm^{-1} and 720 cm^{-1} indicate the existence of aromatic rings. All these signals are evidence for the successful synthesis of PAHN. Determined by *GPC* and *DSC*, the *Mn* of PAHN was approximately 1.4×10^4 and the T_g was 134 °C (Fig. S1), respectively.

3.2. Characterization of protein imprinted polymeric nanoparticles (MIP NPs)

Macromolecular self-assembly was employed to drive the construction of protein imprinted polymeric nanoparticles. We chose BSA as a model protein. The copolymer PAHN was a desirable candidate for the imprinting process, because it had similar amino and hydroxy units to amino acids which could connect the protein scaffold via noncovalent interactions (hydrogen bonding and electrostatic force). This procedure was the critical step for guaranteeing efficient and reversible imprinting between PAHN and the template protein. During the co-assembly process, PAHN chains undergo a transition from random coils into structured nano-assemblies. Meanwhile, the template protein BSA was incorporated into the resultant assemblies via non-covalent interactions. As a result, the imprinted 3D structure was constructed around the template protein to generate binding sites. Non-imprinted polymeric nanoparticles (NIP NPs) without BSA encapsulation were also prepared. The average diameter of MIP NPs was approximately 280 nm (Fig. 2A). The NIP NPs were 230 nm (Fig. 2D) which was approximately 50 nm smaller than MIP NPs. An increased size of MIP NPs was associated with the encapsulation of other molecules [31], which further verified that BSA was successful loaded into MIP NPs. TEM (Fig. 2B) and SEM (Fig. 2C) images showed that spherical-like nanoparticles were observed in MIP, but the size of MIP NPs was larger than NIP (Fig. 2E and F), which was consistent with DLS results.

To further confirm the successful fabrication of MIP NPs, FT-IR spectra were recorded (Fig. 3A). Compared with PAHN, MIP NPs exhibited a distinct peak at 1539 cm^{-1}, and enhanced peaks at 1646 cm^{-1} and 3276 cm^{-1}, which were corresponding to the stretching vibration of the C=O and N–H bond. This coincided with the typical absorption peaks of BSA structure. FT-IR results offered strong evidence for the successful encapsulation of BSA into the resultant MIP NPs.

The far-UV circular dichroism (CD) absorption spectra were recorded to identify the secondary structural stability of BSA (Fig. 3B). Compared to the conventional MIP materials that originated from small-monomers, pre-designed linear macro-monomer was expected to protect the protein's structural integrity. For BSA, there was a typical UV–vis adsorption peak at 200–230 nm due to its helical conformation [32]. The position and strength of negative peak did not change much after encapsulation of BSA into PAHN, which demonstrated that there was almost no effect on BSA conformation and PAHN stabilizes the template commendably. However, the typical broad UV–vis adsorptions dramatically decreased when BSA interacted with small-monomers. That was due to the destructive effect of small-monomers on the secondary structure of BSA. These results revealed that the linear PAHN macromolecule was capable of preservation of protein's secondary structure (Scheme 1).

3.3. Evaluation of MIP electrochemical sensor

The self-assembled MIP NPs used as sensing layer were dropped onto the surface of a polished gold electrode (Scheme 1). As water evaporated, MIP NPs gradually precipitated and accumulated onto the electrode, resulting in formation of an MIP NP layer. The layer then underwent electrochemical polymerization to anchor the imprinted sites and establish a robust electroactive polycarbazole network. Film-forming property of MIP NPs should be satisfactory because the process of electro-polymerization increased the interface bonding between MIP and the substrate [33].

The electro-polymerization of carbazole moieties was achieved using cyclic voltammetry (CV) (Fig. S2A). When the electro-polymerization occurred, an irreversible oxidation peak appeared close to 1.2 V, which was in agreement with the generation of carbazole cation radicals [34]. The C–C dimerization of cation radicals led to a dicarbazyl structure, resulting in a subsequent combination of the carbazole moieties. With sequential 20 repetitive CV

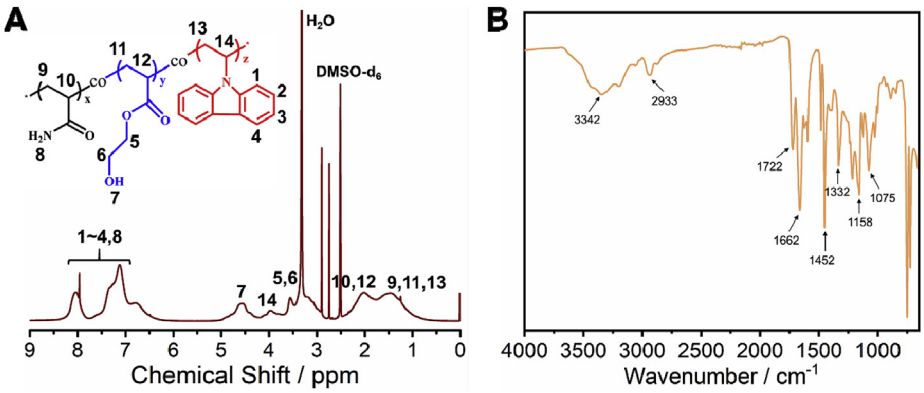

Fig. 1. ^{1}H NMR spectrum (A) and FT-IR spectrum (B) of macro-monomer PAHN.

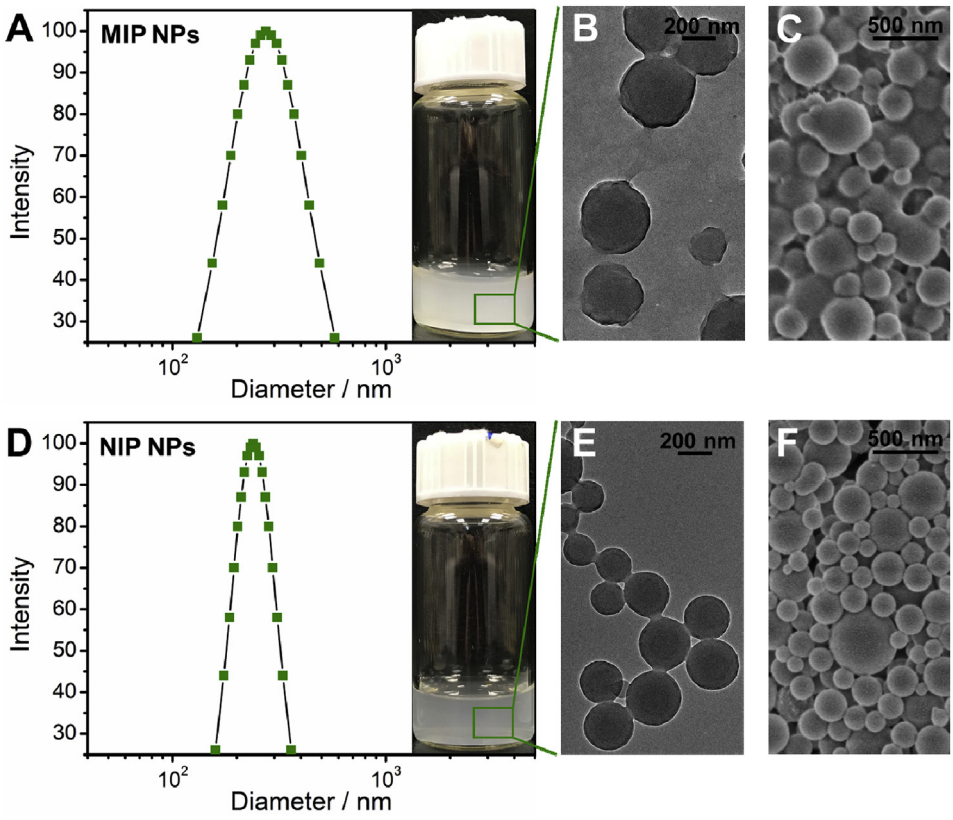

Fig. 2. The diameters, TEM and SEM images of MIP NPs (A, B, C) and NIP NPs (D, E, F). Inset: digital photographs of corresponding dispersion aqueous solution.

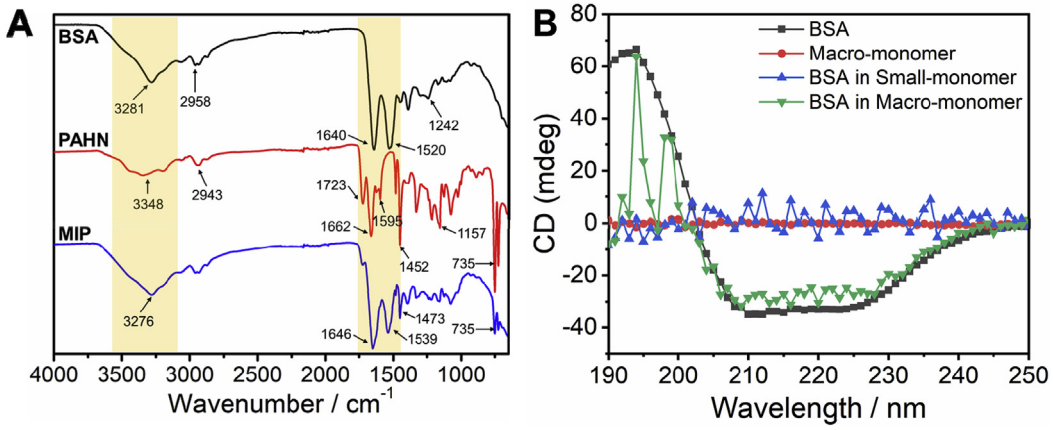

Fig. 3. (A) FT-IR spectra of BSA, PAHN, and MIP NPs. (B) The far-UV CD spectra of BSA, macro-monomer (PAHN), BSA in small-monomers (AM, HEA and NVc) and BSA in macro-monomer.

cycles, the amount of carbazole was consumed. The principal species and reactions in this process were shown in Fig. S2B. As a universal rule, in the electrochemical self-oxidation of carbazole, each step referred to one electron transformation during the rapid coupling reactions [29]. However, in reality, the process of electro-polymerization was more complex for several reactions accompanying the electron transfer. Eventually, a conductive polycarbazole network was created with conjugated cross-linkages between inter- and intramolecular of carbazole groups, which was expected to enhance the electroactivity of MIP layer.

To verify the influence of electroactive network on the MIP sensing platform, CV and electrochemical impedance spectra (EIS) were recorded to trace the process of carbazole self-oxidation polymerization (Fig. 4). With the increase in electro-polymerization cycles, the extent of polymerization increased, as well as the redox peaks of $[Fe(CN)_6]^{3-/4-}$ due to the generation of an electroactive network (Fig. 4A). EIS was recorded to prove the electron transfer ability of the MIP sensing interface (Fig. 4B). In general, an EIS consisted of two portions: a semicircle related to electron-transfer resistance and a linear part corresponding to the diffusion process. A smaller semicircle indicated a decreased electron-transfer resistance. With the increase in electro-polymerization cycle number, the diameter of semicircle part decreased, indicating a significant enhancement of electron transfer ability. After 20 electro-polymerization cycles, there

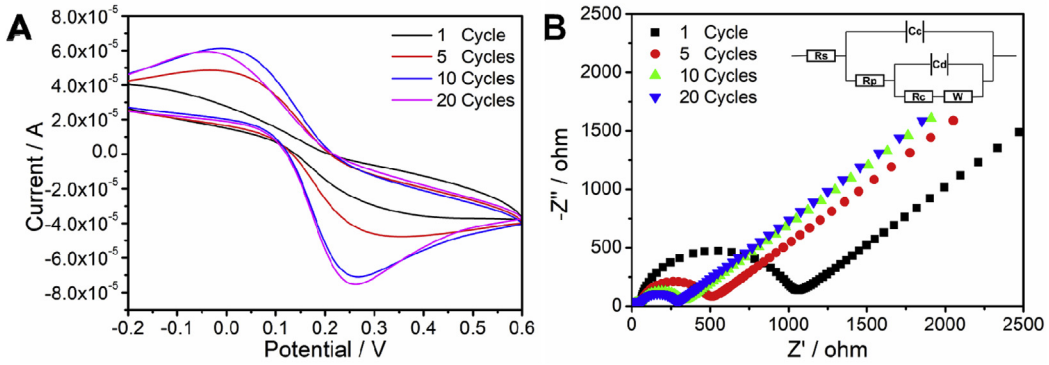

Fig. 4. Cyclic voltammograms (CV) (A) and electrochemical impedance spectra (EIS) (B) of MIP layer after different electro-polymerization cycles. The supporting electrolyte is a solution of $[Fe(CN)_6]^{3-/4-}$ (5 mmol L^{-1}) and KCl (0.2 mol L^{-1}).

was no improvement in electrical performance compared to 10 cycles. Therefore, the number of 20 CV cycles was chosen for electro-polymerization.

SEM was employed to trace the fabrication process (Fig. 5). When the electrode was modified with MIP NPs, there was high accumulation of spherical nanoparticles (Fig. 5B). After electro-polymerization, numerous electroactive polycarbazole particles were generated *in situ* (Fig. 5C). It was expected that the signal conversion of MIP could be improved intrinsically, further enhancing recognition performance. The contact angles of the modified electrode were recorded in Fig. 5D. In comparison to the MIP NP-modified electrode, the contact angle increased after electro-polymerization due to the increased compactness.

Electrochemical behavior was investigated to understand the construction of the MIP sensing interface. Fig. S3A showed the CV voltammograms of different electrodes. After MIP NPs modification, the redox current of $[Fe(CN)_6]^{3-/4-}$ showed an evident decrease due to the shielding efficiency of MIP layer. However, the redox current increased with the generation of electroactive network after electro-polymerization. When the template protein was extracted by an SDS/acetic acid mixture (the process of extraction was shown in Fig. S4), the typical redox currents of $[Fe(CN)_6]^{3-/4-}$ were enhanced further because of the revealed vacant recognition sites. Understandably, EIS curves were consistent with CV, as shown in Fig. S3B.

3.4. Performance of the MIP sensor

Quantificational Recognition of BSA: After the template protein extraction, vacant recognition sites were exposed (Fig. 6A). These sites allowed the diffusion of probe towards the electrode surface, leading to an increased response current. When the sensor was incubated in a template protein solution, the recognition sites could rebind template molecules to inhibit diffusion of the probe towards the electrode surface. Consequently, a current change (ΔI) was observed (Fig. 6A), which was known as "blocking effect" mechanism [35].

To assess selective recognition performance, the fabricated MIP sensor was applied for detecting BSA. After BSA extraction, the sensor was incubated in BSA solution (PBS, pH 7.4) for 6 min (Fig. S5). The response currents were recorded by differential pulse stripping voltammetry (DPSV) in a probe solution. The increased BSA concentration led to a decreased response current (Fig. 6B), indicating that the recognition sites rebound BSA molecules via complementarity in spatial structure and functional group orientation and "blocking effect" worked. Fig. 6C showed an unambiguous linear calibration between ΔI (variation of DPSV response current compared with the blank) and logarithm of BSA concentrations. It revealed a regression equation of $\Delta I\ (\mu A) = 9.716 \log C_{BSA} + 196.95$ ($R^2 = 0.993$) in the range from 10^{-14} to 10^{-5} mg mL^{-1} (1.515×10^{-19} to 1.515×10^{-10} mol L^{-1}). This relationship would rather be exponential than linear for the sensitivity to small concentration differences was higher than that of large concentration differences, indicating a certified sensitivity. The proposed MIP sensor was comparable to previously reported materials for protein recognition (Table 1). Notably, the recognition range was the broadest among all compared BSA sensors. This result revealed that it was one of the most effective strategies to recognize BSA. The excellent performance was mainly owing to a mild procedure for the electrosynthesis of MIP interface to detect fragile proteins. The use of macromonomer well maintained the original structure of protein template, which ensured the availability of fabricated imprinted sites. In addition, the generation of an electroactive network could not only construct a robust MIP layer with good stability, but also facilitate

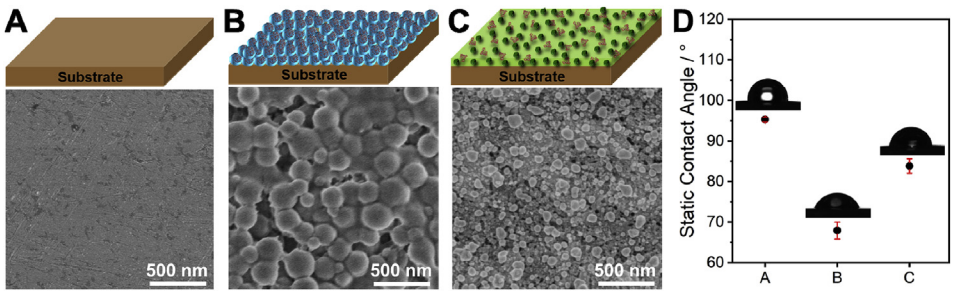

Fig. 5. SEM images of bare electrode (A), MIP NP-modified electrode (B), and MIP NP-modified electrode after electro-polymerization (C). (D) corresponding contact angles of A, B, and C electrodes.

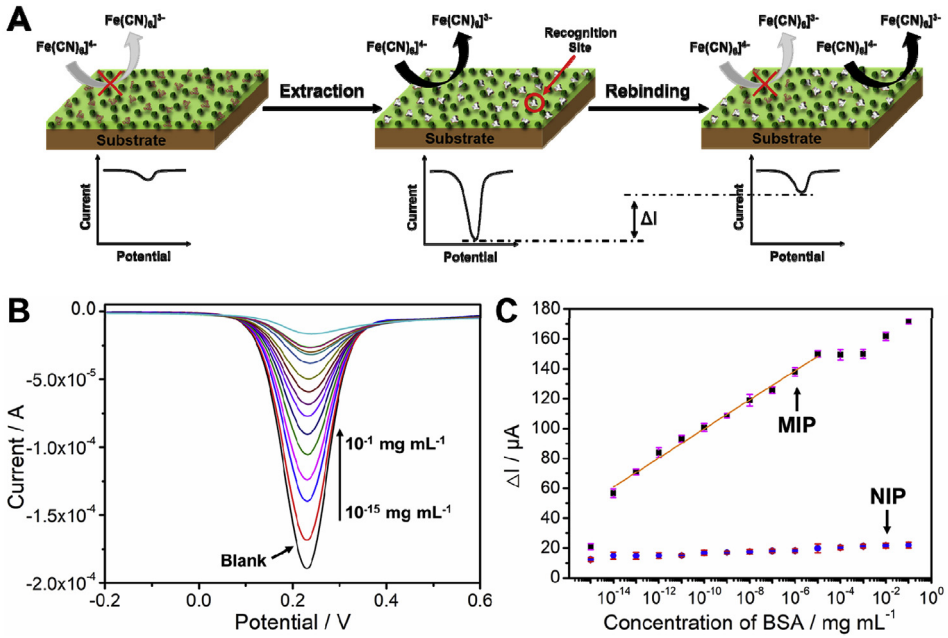

Fig. 6. (A) Schematic of the fabrication and recognition mechanism of MIP sensing interface. DPSV curves (B) and linear calibration (C) between ΔI and logarithm value of BSA concentrations on MIP sensor and NIP sensor. The supporting electrolyte is a PBS (pH 7.4) solution containing probe $[Fe(CN)_6]^{3-/4-}$.

intrinsic electronic transmission.

By contrast, no significant current changes were observed for NIP sensor following an increase in BSA concentration (Fig. 6C), which further indicated that the electrochemical responses were exclusively caused by the recognition reaction between imprinted sites and template protein. Imprinting factor (IF) was calculated according to the equation $IF = \Delta I_{MIP}/\Delta I_{NIP}$, where ΔI_{MIP} and ΔI_{NIP} were the response currents of MIP and NIP with maximum response concentrations. A high IF value of 8.45 was obtained, which revealed that there was significant availability of the proposed material for protein detection.

Selectivity, Stability and Reproducibility of the MIP Sensor: The selectivity of the proposed MIP sensor was evaluated by using other analogues, including tryptophan (Tryp), L-glutamic acid (Glu), lysine (Lys), glycine (Gly), trypsin, ovalbumin (OVA), and bovine hemoglobin (BHB). The responses on the MIP sensor for all concentrations were recorded (Fig. 7A). As shown, the current variations of these analogues were negligible in comparison to BSA. The IF values were calculated as Tryp (1.03), Lys (1.01), Glu (1.13), Gly (1.09), OVA (2.09), and BHB (2.38), which were much lower than that of BSA.

The electrochemical responses every few days were recorded to investigate the long-term stability of the MIP sensor (Fig. 7B). There was no obvious variation in response current after 9 days, and the sensor retained approximately 90% of initial value after 1 month.

Table 1
Sensing performance comparison with previous works for BSA detection.

Materials	Linear range (mg mL^{-1})	References
Magnetic NPs/CNTs	10^{-7}–10^{-1}	[36]
MIP/ionic liquid-graphene composite	10^{-10}–10^{-4}	[37]
Paper with graphite-based ink	10^{-3}–10^{2}	[38]
Epitope-based MIP/HRP	10^{-6}–1.50×10^{-4}	[39]
MIP	10^{-5}–5×10^{-3}	[40]
MIP/WCNTs	10^{-4}–10^{-2}	[41]
MIP/CdTe quantum dots	3.3×10^{-2}–6.6×10^{-1}	[42]
Temperature-sensitive MIP	$\approx 2 \times 10^{-5}$–10^{-2}	[43]
Electroactive MIP	10^{-14}–10^{-5}	This work

Therefore, all measurements in the blank or samples should be taken soon to avoid errors caused by signal weakening. The result indicated that the immobilized recognition sites retained stability for long durations. To test the reproducibility, five MIP sensors were independently constructed via the same preparation procedure. After template extraction, DPSV currents were obtained (Fig. 7C). It showed a relative standard deviation (R.S.D.) of 6.8%, which indicated a satisfactory reproducibility.

3.5. General applicability of the proposed approach

Trypsin, an important protease in human, is a hydrolytic enzyme secreted by the pancreas. In a clinical setting, a trypsin assay can be used to predict and diagnose pancreatic diseases [44]. The concentration of trypsin varies in different parts of the body under normal conditions, for example, 150–600 μg mL^{-1} in duodenal juice, and almost zero in the urine. Therefore, trypsin was chosen as an additional model protein in the present study. TEM image of trypsin imprinted polymeric nanoparticles revealed that the assembled nanoparticles were spherical-like shapes with an average diameter of 350 nm (Fig. 8A). Far-UV CD absorption spectra were also recorded to identify the secondary structural stability of trypsin in the macromonomer PAHN (Fig. 8B). In terms of trypsin in PAHN, the strength and position of broad UV–vis adsorption peak were consistent with pure trypsin, which demonstrated that the conformation of trypsin in PAHN was well maintained. Using the same preparation procedure, a trypsin imprinted sensor was fabricated (Fig. S6). After incubation in different trypsin concentrations, DPSV responses were recorded (Fig. 8C). The resulting calibration was shown in Fig. 8D. The sensor demonstrated a well-defined dependence on the logarithm of trypsin concentrations with linear responses in 10^{-13}–10^{-8} mg mL^{-1} (4.166×10^{-18}–4.166×10^{-13} mol L^{-1}) (ΔI (μA) = $0.10 \log C_{Trypsin} + 3.97$, $R^2 = 0.998$). The selectivity of the trypsin imprinted sensor was evaluated in Fig. S7. The response current of trypsin was much higher than that of interferents, and the added interferents did not have obvious effect. These performance results were strong evidence that the approach presented in this work was one of most effective

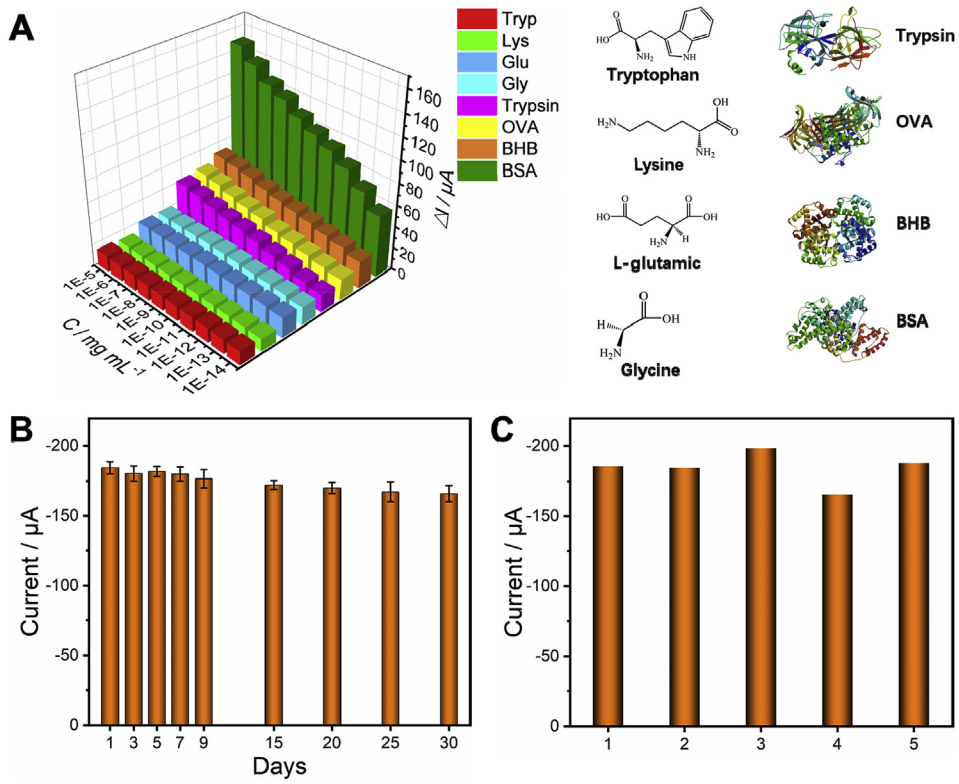

Fig. 7. (A) Current responses on MIP sensor for different concentrations of tryptophan (Tryp), Lys (lysine), L-glutamic acid (Glu), glycine (Gly), trypsin, ovalbumin (OVA), bovine hemoglobin (BHB) and BSA, and the structures of Tryp, Lys, Gly, Glu, trypsin, OVA, BHB and BSA. (B) DPSV currents of one MIP sensor after template extraction every few days. (C) DPSV currents of different MIP sensors after template extraction. All data were recorded in a PBS (pH 7.4) solution containing $[Fe(CN)_6]^{3-/4-}$ as probe.

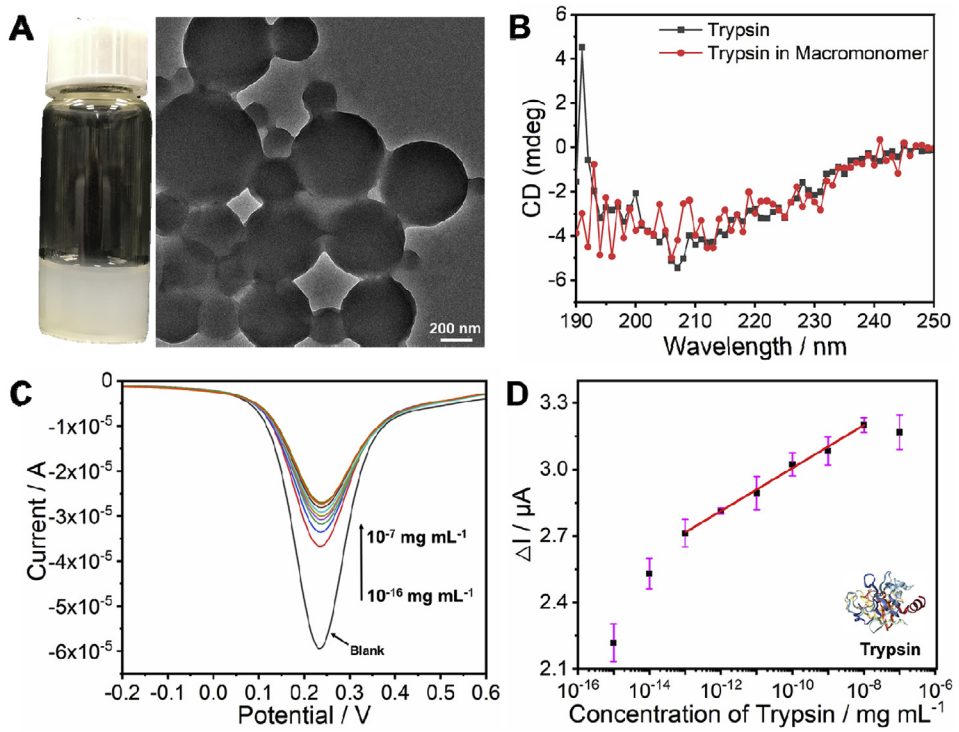

Fig. 8. (A) TEM image of trypsin imprinted nanoparticles. (B) The far-UV CD spectra of trypsin and trypsin in macro-monomer PAHN. DPSV curves (C) and linear calibration (D) between ΔI and logarithm value of trypsin concentrations on MIP sensor.

Table 2
Sensing performance comparison with previous works for trypsin detection.

Materials	Linear range (mg mL^{-1})	References
Surface-imprinted PDA sensor	$\approx 2.4 \times 10^{-5}$–$1.2 \times 10^{-3}$	[45]
Colorimetric sensor	5.0×10^{-6}–2.0×10^{-3}	[46]
Fluorescence sensor	0.2×10^{-3}–0.1	[47]
Colorimetric sensor	6×10^{-5}–6×10^{-4}	[48]
Fluorescence resonance energy transfer biosensor	2.5×10^{-6}–8×10^{-5}	[49]
Fluorescent probe	~4×10^{-4}	[50]
Upconversion nanoparticles	5×10^{-6}–8×10^{-5}	[51]
Electroactive MIP	10^{-13}–10^{-8}	This work

strategies to recognize trypsin compared with previous reports (Table 2). The successful electrochemical determination of trypsin suggested that the presented approach had the potential to be detect other biomacromolecules.

In order to demonstrate the ability of real sample analysis, the MIP sensor was applied to detect trypsin in human urine which was collected from a healthy individual. It showed that trypsin could not be found in normal human urine. Then the recovery experiment has been done in Table S1. The obtained RSD% was less than 8%, which confirmed that the MIP sensor can be used for practical sample analysis.

4. Conclusions

In the present study, a high-efficiency MIP sensing platform has been conducted to recognize protein by employing a linear electropolymerizable macro-monomer. Self-assembly of the linear macromonomer was expected to protect the protein's structural integrity. BSA and trypsin were employed as biomacromolecular templates to fabricate MIP NPs. As a proof of principle, the MIP NPs were immobilized on an electrode, and electro-polymerization was used to generate an electroactive network. After template removal, a high-performance MIP sensing interface was formed for electrochemical protein recognition. Results demonstrated that it was one of most effective strategies to recognize protein such as BSA and trypsin. It offered an adaptable fabrication of electroactive MIP sensor as an abiotic recognitiEon platform.

Declaration of competing interest

The authors declare that they have no known competing financial interests or personal relationships that could have appeared to influence the work reported in this paper.

CRediT authorship contribution statement

Wei Zhao: Conceptualization, Methodology, Formal analysis, Investigation, Writing - original draft, Data curation, Visualization. **Bing Li:** Methodology, Investigation, Data curation, Visualization. **Sheng Xu:** Methodology, Investigation, Visualization. **Ye Zhu:** Validation, Conceptualization, Funding acquisition. **Xiaoya Liu:** Conceptualization, Validation, Writing - review & editing, Project administration, Supervision, Funding acquisition.

Acknowledgements

The authors would like to thank the National Natural Science Foundation of China (51803079, 51573073), the Postgraduate Research & Practice Innovation Program of Jiangsu Province (KYCX19_1850), International Joint Research Center for Photoresponsive Molecules and Materials, and MOE & SAFEA for the 111 Project (B13025).

Appendix A. Supplementary data

Supplementary data to this article can be found online at https://doi.org/10.1016/j.aca.2020.04.023.

References

[1] J. Aizenberg, P. Fratzl, Biological and biomimetic materials, Adv. Mater. 21 (4) (2009) 387–388.
[2] S. Vignolini, N. Bruns, Bioinspiration across all length scales of materials, Adv. Mater. 30 (19) (2018) 1801687–1801690.
[3] E.B. Lavik, G. Zheng, Biomimetic materials, Bioconjugate Chem. 29 (2018), 825-825.
[4] E. Persch, O. Dumele, F. Diederich, Molecular recognition in chemical and biological systems, Angew. Chem. Int. Ed. 54 (11) (2015) 3290–3327.
[5] T.B. Wu, X.J. Xiao, Z. Zhang, M.P. Zhao, Enzyme-mediated single-nucleotide variation detection at room temperature with high discrimination factor, Chem. Sci. 6 (2015) 1206–1211.
[6] G.C. Yu, K.C. Jie, F.H. Huang, Supramolecular amphiphiles based on host–guest molecular recognition motifs, Chem. Rev. 115 (15) (2015) 7240–7303.
[7] D.E. Hansen, Recent developments in the molecular imprinting of proteins, Biomaterials 28 (29) (2007) 4178–4191.
[8] L.X. Chen, S.F. Xu, J.H. Li, Recent advances in molecular imprinting technology: current status, challenges and highlighted applications, Chem. Soc. Rev. 40 (5) (2011) 2922–2942.
[9] G. Wulff, Enzyme-like catalysis by molecularly imprinted polymers, Chem. Rev. 102 (1) (2002) 1–28.
[10] M. Resmini, Molecularly imprinted polymers as biomimetic catalysts, Anal. Bioanal. Chem. 402 (10) (2012) 3021–3026.
[11] D.L. Huang, R.Z. Wang, Y.G. Liu, G.M. Zeng, C. Lai, P. Xu, B.A. Lu, J.J. Xu, C. Wang, C. Huang, Application of molecularly imprinted polymers in wastewater treatment: a review, Environ. Sci. Pollut. Res. 22 (2) (2015) 963–977.
[12] A. Sarafraz-Yazdi, N. Razavi, Application of molecularly-imprinted polymers in solid-phase microextraction techniques, Trac. Trends Anal. Chem. 73 (2015) 81–90.
[13] F. Puoci, G. Cirillo, M. Curcio, O.I. Parisi, F. Iemma, N. Picci, Molecularly imprinted polymers in drug delivery: state of art and future perspectives 8 (10) (2011) 1379–1393.
[14] A.G. Ayankojo, J. Reut, R. Boroznjak, A. Öpik, V. Syritski, Molecularly imprinted poly (meta-phenylenediamine) based QCM sensor for detecting Amoxicillin, Sensor. Actuator. B Chem. 258 (2018) 766–774.
[15] C. Yang, X.F. Ji, W.Q. Cao, J. Wang, Q. Zhang, T.L. Zhong, Y. Wang, An ultra sensitive and selective impedance sensor based on protein-imprinted polymer, Sensor. Actuator. B Chem. 282 (2019) 818–823.
[16] M.J. Abdin, Z. Altintas, I.E. Tothill, In silico designed nanoMIP based optical sensor for endotoxins monitoring, Biosens. Bioelectron. 67 (2015) 177–183.
[17] F. Canfarotta, J. Czulak, K. Betlem, A. Sachdeva, K. Eersels, B. van Grinsven, T.J. Cleij, M. Peeters, A novel thermal detection method based on molecularly imprinted nanoparticles as recognition elements, Nanoscale 10 (4) (2018) 2081–2089.
[18] L.W. Qian, X.L. Hu, P. Guan, D. Wang, J. Li, C.B. Du, R.Y. Song, C.L. Wang, W.Q. Song, The effectively specific recognition of bovine serum albumin imprinted silica nanoparticles by utilizing a macromolecularly functional monomer to stabilize and imprint template, Anal. Chim. Acta 884 (2015) 97–105.
[19] W.H. Zhou, C.H. Lu, X.C. Guo, F.R. Chen, H.H. Yang, X.R. Wang, Mussel-inspired molecularly imprinted polymer coating superparamagnetic nanoparticles for protein recognition, J. Mater. Chem. 20 (5) (2010) 880–883.
[20] R.N. Liang, J.W. Ding, S.S. Gao, W. Qin, Mussel-inspired surface-imprinted sensors for potentiometric label-free detection of biological species, Angew. Chem. Int. Ed. 56 (24) (2017) 6833–6837.
[21] R. Tchinda, A. Tutsch, B. Schmid, R.D. Süssmuth, Z. Altintas, Recognition of protein biomarkers using epitope-mediated molecularly imprinted films: histidine or cysteine modified epitopes, Biosens. Bioelectron. 123 (2019) 260–268.
[22] M.D. Attieh, Y. Zhao, A. Elkak, A. Falcimaigne-Cordin, K. Haupt, Enzyme-initiated free-radical polymerization of molecularly imprinted polymer

nanogels on a solid phase with an immobilized radical source, Angew. Chem. 129 (12) (2017) 3387–3391.
[23] W. Zhao, R.L. Zhang, S. Xu, J. Cai, X.J. Zhu, Y. Zhu, W. Wei, X.Y. Liu, J. Luo, Molecularly imprinted polymeric nanoparticles decorated with Au NPs for highly sensitive and selective glucose detection, Biosens. Bioelectron. 100 (2018) 497–503.
[24] S. Xu, G.Y. Lin, W. Zhao, Q. Wu, J. Luo, W. Wei, X.Y. Liu, Y. Zhu, Necklace-like molecularly imprinted nanohybrids based on polymeric nanoparticles decorated multiwalled carbon nanotubes for highly sensitive and selective melamine detection, ACS Appl. Mater. Interfaces 10 (29) (2018) 24850–24859.
[25] P.N. Bartlett, F.A. Al-Lolage, There is no evidence to support literature claims of direct electron transfer (DET) for native glucose oxidase (GOx) at carbon nanotubes or graphene, J. Electroanal. Chem. 819 (2018) 26–37.
[26] Y. Ofir, B. Samanta, V.M. Rotello, Polymer and biopolymer mediated self-assembly of gold nanoparticles, Chem. Soc. Rev. 37 (9) (2008) 1814–1825.
[27] T.O. Mason, U. Shimanovich, Fibrous protein self-Assembly in biomimetic materials, Adv. Mater. 30 (41) (2018) 1706462–1706473.
[28] A. Bossi, F. Bonini, A.P.F. Turner, S.A. Piletsky, Molecularly imprinted polymers for the recognition of proteins: the state of the art, Biosens. Bioelectron. 22 (6) (2007) 1131–1137.
[29] G. Inzelt, Formation and redox behaviour of polycarbazole prepared by electropolymerization of solid carbazole crystals immobilized on an electrode surface, J. Solid State Electrochem. 7 (8) (2003) 503–510.
[30] J.L. Liu, J.Z. Ma, Y. Bao, J. Wang, Z.F. Zhu, H.R. Tang, L.M. Zhang, Nanoparticle morphology and film-forming behavior of polyacrylate/ZnO nanocomposite, Compos. Sci. Technol. 98 (2014) 64–71.
[31] B.G. Yu, T. Okano, K. Kataoka, G. Kwon, Polymeric micelles for drug delivery: solubilization and haemolytic activity of amphotericin B, J. Contr. Release 53 (1–3) (1998) 131–136.
[32] W. Zhao, B. Li, S. Xu, X.W. Huang, J. Luo, Y. Zhu, X.Y. Liu, Electrochemical protein recognition based on macromolecular self-assembly of molecularly imprinted polymer: a new strategy to mimic antibody for label-free biosensing, J. Mater. Chem. B 7 (14) (2019) 2311–2319.
[33] F.C. Krebs, Fabrication and processing of polymer solar cells: a review of printing and coating techniques, Sol. Energy Mater. Sol. Cell. 93 (4) (2009) 394–412.
[34] M. Baibarac, M. Lira-Cantú, J. Oró Sol, I. Baltog, N. Casañ-Pastor, P. Gomez-Romero, Poly (N-vinyl carbazole) and carbon nanotubes based composites and their application to rechargeable lithium batteries, Compos. Sci. Technol. 67 (11–12) (2007) 2556–2563.
[35] M. Pawlak, G. Mistlberger, E. Bakker, Concanavalin A electrochemical sensor based on the surface blocking principle at an ion-selective polymeric membrane, Microchim. Acta 182 (1–2) (2015) 129–137.
[36] H.J. Chen, Z.H. Zhang, L.J. Luo, S.Z. Yao, Surface-imprinted chitosan-coated magnetic nanoparticles modified multi-walled carbon nanotubes biosensor for detection of bovine serum albumin, Sensor. Actuator. B Chem. 163 (1) (2012) 76–83.
[37] J.F. Xia, X.Y. Cao, Z.H. Wang, M. Yang, F.F. Zhang, B. Lu, F. Li, L. Xia, Y.H. Li, Y.Z. Xia, Molecularly imprinted electrochemical biosensor based on chitosan/ionic liquid–graphene composites modified electrode for determination of bovine serum albumin, Sensor. Actuator. B Chem. 225 (2016) 305–311.
[38] N.S. Ferreira, A.P.T. Moreira, M.H.M. de Sá, M.G.F. Sales, New electrochemically-derived plastic antibody on a simple conductive paper support for protein detection: application to BSA, Sensor. Actuator. B Chem. 243 (2017) 1127–1136.
[39] M.X. Li, X.H. Wang, L.M. Zhang, X.P. Wei, A high sensitive epitope imprinted electrochemical sensor for bovine serum albumin based on enzyme amplifying, Anal. Biochem. 530 (2017) 68–74.
[40] J.H. Yu, F.W. Wan, C.C. Zhang, M. Yan, X.N. Zhang, S.W. Wang, Molecularly imprinted polymeric microspheres for determination of bovine serum albumin based on flow injection chemiluminescence sensor, Biosens. Bioelectron. 26 (2) (2010) 632–637.
[41] Y.Y. Wang, M. Han, G.S. Liu, X.D. Hou, Y.N. Huang, K.B. Wu, C.Y. Li, Molecularly imprinted electrochemical sensing interface based on in-situ-polymerization of amino-functionalized ionic liquid for specific recognition of bovine serum albumin, Biosens. Bioelectron. 74 (2015) 792–798.
[42] Y. Wang, Q.Z. Hu, T.T. Tian, Y.A. Gao, L. Yu, A nonionic surfactant-decorated liquid crystal sensor for sensitive and selective detection of proteins, Anal. Chim. Acta 937 (2016) 119–126.
[43] Y.B. Wei, Q. Zeng, Q. Hu, M. Wang, J. Tao, L.S. Wang, Self-cleaned electrochemical protein imprinting biosensor basing on a thermo-responsive memory hydrogel, Biosens. Bioelectron. 99 (2018) 136–141.
[44] G. Ertürk, M. Hedström, B. Mattiasson, A sensitive and real-time assay of trypsin by using molecular imprinting-based capacitive biosensor, Biosens. Bioelectron. 86 (2016) 557–565.
[45] R.N. Liang, J.W. Ding, S.S. Gao, W. Qin, Mussel-inspired surface-imprinted sensors for potentiometric label-free detection of biological species, Angew. Chem. Int. Ed. 56 (24) (2017) 6833–6837.
[46] L.F. Zhang, J.X. Du, A sensitive and label-free trypsin colorimetric sensor with cytochrome c as a substrate, Biosens. Bioelectron. 79 (2016) 347–352.
[47] H.X. Li, M.M. Yang, D.S. Kong, R. Jin, X. Zhao, F.M. Liu, X. Yan, Y.H. Lin, G.Y. Lu, Sensitive fluorescence sensor for point-of-care detection of trypsin using glutathione-stabilized gold nanoclusters, Sensor. Actuator. B Chem. 282 (2019) 366–372.
[48] X.Y. Lin, Z.M. Zhu, C.F. Zhao, S.G. Li, Q.C. Liu, A.L. Liu, L.Q. Lin, X.H. Lin, Robust oxidase mimicking activity of protamine-stabilized platinum nanoparticles units and applied for colorimetric sensor of trypsin and inhibitor, Sensor. Actuator. B Chem. 284 (2019) 346–353.
[49] S.M. Xu, F.M. Zhang, L.B. Xu, X. Liu, P.Y. Ma, Y. Sun, X.H. Wang, D.Q. Song, A fluorescence resonance energy transfer biosensor based on carbon dots and gold nanoparticles for the detection of trypsin, Sensor. Actuator. B Chem. 273 (2018) 1015–1021.
[50] S.S. Huang, F.F. Li, C.Y. Liao, B.Z. Zheng, J. Du, D. Xiao, A selective and sensitive fluorescent probe for the determination of HSA and trypsin, Talanta 170 (2017) 562–568.
[51] H.Y. Chen, A.J. Fang, Y.Y. Zhang, S.Z. Yao, Silver triangular nanoplates as an high efficiently FRET donor-acceptor of upconversion nanoparticles for ultrasensitive “Turn on-off” protamine and trypsin sensor, Talanta 174 (2017) 148–155.